Chapter

# Application of UAV Remote Sensing in Monitoring Banana Fusarium Wilt

*Huichun Ye, Wenjiang Huang, Shanyu Huang, Chaojia Nie, Jiawei Guo and Bei Cui*

## Abstract

Fusarium wilt poses a current threat to worldwide banana plantation areas. To treat the Fusarium wilt disease and adjust banana planting methods accordingly, it is important to introduce timely monitoring processes. In this chapter, the multispectral images acquired by unmanned aerial vehicle (UAV) was used to establish a method to identify which banana regions were infected or uninfected with Fusarium wilt disease. The vegetation indices (VIs), including the normalised difference vegetation index (NDVI), normalised difference red edge index (NDRE), structural independent pigment index (SIPI), red-edge structural independent pigment index ($SIPI_{RE}$), green chlorophyll index ($CI_{green}$), red-edge chlorophyll index ($CI_{RE}$), anthocyanin reflectance index (ARI), and carotenoid index (CARI), were selected for deciding the biophysical and biochemical characteristics of the banana plants. The relationships between the VIs and those plants infected or uninfected with Fusarium wilt were assessed using the binary logistic regression method. The results suggest that UAV-based multispectral imagery with a red-edge band is effective to identify banana Fusarium wilt disease, and that the CIRE had the best performance.

**Keywords:** Fusarium wilt, banana, UAV, remote sensing

## 1. Introduction

Bananas (*Musa spp.*) are a widely cultivated cash crop in both the tropical and subtropical regions. Caused by the soilborne fungus *Fusarium oxysporum* f. sp. *cubense* (*Foc*), Banana Fusarium wilt (also known as Panama disease) seriously threatens global banana cultivation and export [1, 2]. As reported, banana Fusarium wilt may have affected up to 100,000 hectares of banana plantations. Moreover, it continues to spread, through infected plant materials and contaminated soil and flowing water, or through farm machinery and inappropriate sanitation measures [2]. Externally, the first sign that a plant is infected with the disease is the withered plant, with the old leaves turning yellow on the edge. With the progression of the disease, the leaves eventually droop and form a 'skirt' around the pseudo-stem before finally falling off. The new leaves may show irregular and wrinkled blades as well as pale margins [3]. Currently, no effective chemical

treatment method has been proposed to control Fusarium wilt. "Removal in time" is the optimal way to prevent the disease spread once a diseased plant is identified [4].

For treatment of the disease, and for crop planting adjustments, real-time monitoring and effective identification of banana Fusarium wilt play a significant role [5]. Traditionally, soil investigations have been the only effective means to monitor crop diseases, but such surveys take a lot of time and are often expensive. Recent years have witnessed the rapid development of the remote sensing technology, which has developed into a viable method for disease assessment and monitoring. The leaf pigment content, leaf area index (LAI) and water content of a plant which is infected with a disease will all undergo changes. And such biochemical and biophysical changes in the plant will also present in its spectral reflectance characteristics [6]. Remote sensing technology has been applied to monitor diseases, including Fusarium head blight [7, 8], rust infection [9–11], and powdery mildew [7, 8, 12, 13] in wheat, grey leaf spot in maize [14], bacterial leaf blight in rice [15, 16], and late blight disease and bacterial spot in tomatoes [17, 18] in some studies. However, the sensitivity of spectral bands and VIs varies with the category of diseases. For example, Bravo et al. [19] calculated the normalised difference vegetation index (NDVI) using wavelengths of 620–640 nm and 740–760 nm for extracting powdery mildew from wheat patches. Devadas et al. [20] distinguished yellow rusted wheat from healthy wheat using the anthocyanin reflection index (ARI). Huang et al. [10] suggested that the position of the red edge can be used as a disease indicator. With this in mind, it is of essence to identify which spectral bands and VIs are suitable for the identification of which specific diseases.

UAV remote sensing technology has been developed rapidly over recent years. It has become of interest due to its advantages of long flight time, real-time image transmission, effective detection of high-risk areas, low cost and easy manoeuvrability. It provides new means for the timely and non-destructive extraction of infected plants from the in-season crops [21]. Using UAV multispectral and hyperspectral images, a great number of studies have achieved significant progress in growth monitoring, crop classification, and the identification of diseases and insect pests [22–24]. Within banana production, a few studies have adopted UAV-based images to map the spatial patterns of photosynthetic activity in banana plantations [25]. Nonetheless, there are few studies that use UAV-based remote sensing to monitor banana Fusarium wilt [26, 27]. Furthermore, the spatial scale for remote sensing information and scaling remains one of the fundamental problems in geoscience [28]. Selecting an optimal spatial scale for remote sensing imagery plays a significant role in agricultural monitoring in particular.

Therefore, the goals of this chapter are to: (i) develop an identification method for Fusarium wilt based on UAV multispectral remote sensing, (ii) determine the optimal VI needed for the establishment of a quality identification model, and (iii) evaluate how different image resolutions affect the accuracy of Fusarium wilt identification in order to provide guidance for the application of satellite-based data in a massive scale.

## 2. Materials and methods

### 2.1 Field experiment

The experiments were carried out at two experimental locations in Guangxi and Hainan, respectively.

The Guangxi experiment site is located in Guangxi Province of China (23°7′53″ to 23°8′4″ N, 107°43′45 to 107°44′7″ E) (**Figure 1**). It has a subtropical monsoon

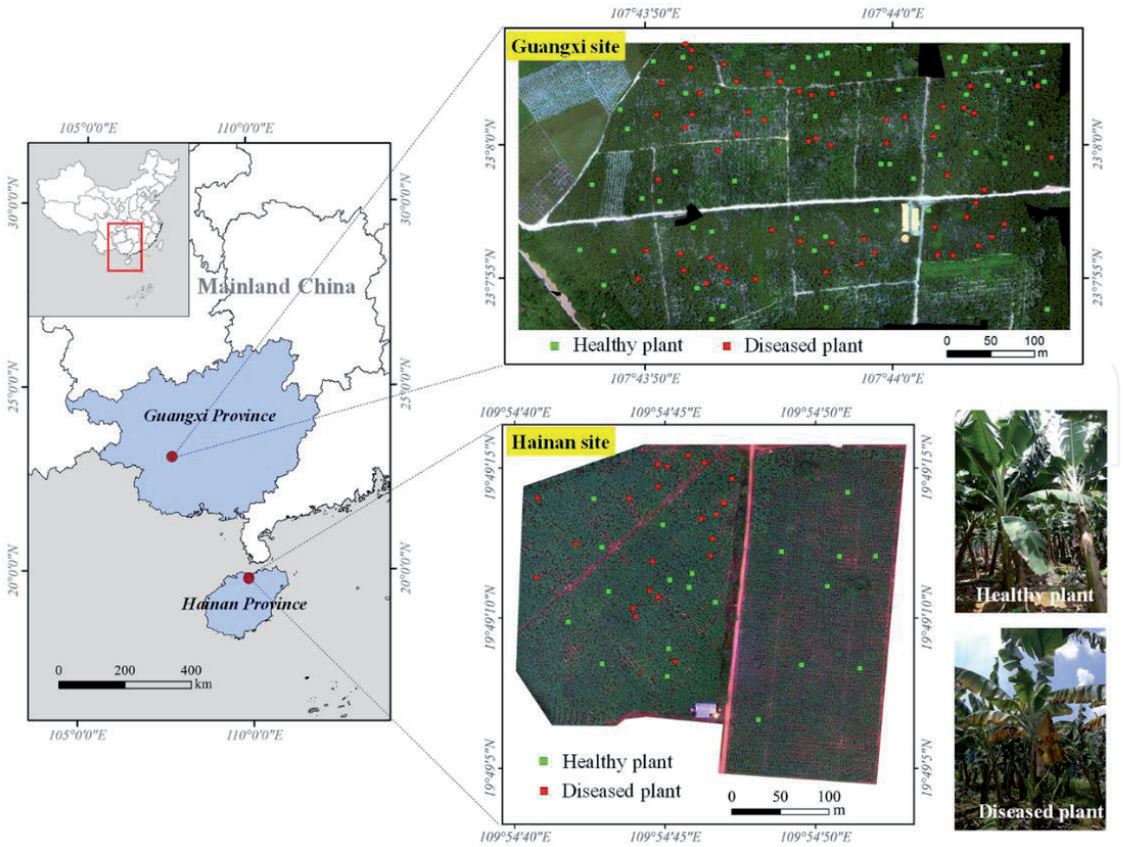


**Figure 1.**
*Location of the experimental sites with the survey sites.*

climate characterised by year-round sunshine and rainfall, with a mean annual temperature between 20.8 to 22.4°C, and an average annual rainfall of 1200 mm. The soil type according to the FAO soil classification system is Ferralsol [29]. The banana variety in the study area was "Williams B6". The leaf number of this variety is 34–36, the plant height is about 2.4–3 m, and the growth period is 10–12 months. The banana plantation was established in September 2015, with the planting distance of 2.0 m by 2.6 m. The first harvest was carried out in November 2016. As of August 2018 (the time of the field investigation discussed in this chapter), the third generation of bananas was in the fields and more than 40% of the banana plants were infected with Fusarium wilt.

The Hainan experiment site is located in Hainan Province, China (19°49′4″ to 19°49′16″ N, 109°54′40″ to 109°54′53″ E) (**Figure 1**). It has a tropical monsoon climate characterised by year-round sunshine and rainfall, with a mean annual temperature between 23.1 to 24.5°C and an average annual rainfall of 1750 mm. The soil type according to the FAO soil classification system is Humic Acrisol [29]. This experimental field was divided into two sub-fields (left area and right area) with the middle road as the boundary (**Figure 1**). The left area was developed in June 2017, with the planting distance of 2.0 m by 2.3 m. The first harvest was carried out in July 2018. The banana variety was "Baxijiao". the plant height of this variety is about 2.6–3.2 m and the growth period is 9–12 months. In this field, the rate of banana Fusarium wilt infection was about 10%.

The right area was developed in August 2018. The planting distance was the same as that in the left field. The banana variety was "Nantianhuang". The plant height of this variety is about 2.5–3.0 m and the growth period is 10–13 months. At the time of the field investigation in December 2018, no banana plants were found to be infected with Fusarium wilt.

In this chapter, the experimental data obtained from the Guangxi site was used for calibration and validation of the Fusarium wilt identification model, and from the Hainan site used for model validation.

## 2.2 Field investigation

### *2.2.1 Plant investigation*

The experiment at Guangxi site was carried out on August 7, 2018. A total of 120 sample plots were investigated to assess the occurrence or non-occurrence of Fusarium wilt (**Figure 1**). Among them, there were 57 healthy samples and 63 diseased samples. The size of each sample plot encompassed one banana plant. Eventually, 75% samples were randomly extracted and employed for the construction of Fusarium wilt identification model denoted by modelling dataset (MD); and the remaining 25% for model validation, denoted by validation dataset 1 (VD1). The experiment at Hainan site was performed on December 11, 2018. The survey strategy was in line with that of the experiment at Guangxi site. A total of 35 sample plots were finally investigated, of which 16 were healthy and 19 were diseased. All the sample plots from Hainan sties were served for model validation, denoted by validation dataset 2 (VD2).

### *2.2.2 UAV multispectral imagery acquisition*

The surveys were carried out by a DJI Phantom 4 Pro quadcopter (DJI Innovations, Shenzhen, China) equipped a MicaSense RedEdge-M multispectral camera (MicaSense, Inc., Seattle, WA, USA). The camera is configured with five bands: Blue (475 nm center, 20 nm bandwidth), Green (560 nm center, 20 nm bandwidth), Red (668 nm center, 10 nm bandwidth), Red edge (717 nm center, 10 nm bandwidth), Near-IR (840 nm center, 40 nm bandwidth). The flight experiment at the Guangxi site was performed between 12:30 p.m.–13:30 p.m. on 7 August 2018, covering an area of 21 ha. While the flight experiment at the Hainan site was implemented between 11:00 a.m.–12:00 p.m. on December11, 2018, covering an area of 11 hectares. The flight altitude above ground level was 120 m with an 8 cm ground sample distance (GSD). Then, the original UAV imagery was resampled to generate images with five resolutions (i.e., 0.5-m, 1-m, 2-m, 5-m, and 10-m) by using nearest neighbour resampling algorithm.

## 2.3 Data analysis

### *2.3.1 Vegetation indices*

In this section, the VIs method was applied to assess the infection status of Fusarium wilt in banana plantations. Eight VIs that related to plant growth and pigment absorption were selected to characterise the biophysical and biochemical variations due to individual infections. These VIs included the NDVI, normalised difference red edge index (NDRE), structural independent pigment index (SIPI), red-edge structural independent pigment index ($SIPI_{RE}$), green chlorophyll index ($CI_{green}$), red-edge chlorophyll index ($CI_{RE}$), anthocyanin reflectance index (ARI), and carotenoid index (CARI). **Table 1** lists the formulations of the VIs.

### *2.3.2 Statistics analysis*

The binary logistic regression (BLR) was used to established the relationships between the VIs and the plants infected or uninfected with Fusarium wilt. As one

| VI | Formulation | Sensitive Parameter | Reference |
|---|---|---|---|
| NDVI | $(R_{NIR}–R_{red})/(R_{NIR} + R_{red})$ | Green biomass, LAI | [30] |
| NDRE | $(R_{NIR}–R_{RE})/(R_{NIR} + R_{RE})$ | Green biomass, LAI | [31] |
| SIPI | $(R_{NIR}–R_{blue})/(R_{NIR} – R_{red})$ | Leaf pigment content | [32] |
| $SIPI_{RE}$ | $(R_{RE}–R_{blue})/(R_{RE} – R_{red})$ | Leaf pigment content | [33] |
| $CI_{green}$ | $R_{NIR}/R_{green}–1$ | Leaf chlorophyll content | [34] |
| $CI_{RE}$ | $R_{NIR}/R_{RE}–1$ | Leaf chlorophyll content | [35] |
| ARI | $1/R_{green}–1/R_{RE}$ | Leaf anthocyanin content | [36] |
| CARI | $R_{RE}/R_{green}–1$ | Leaf carotenoid content | [37] |

**Table 1.**
*List of the VIs used in this chapter.*

of the most common multivariate analysis methods, BLR has a dependent variable as a binary variable that represents the presence or absence of an event. The BLR dependent variable is a probability function, which can be expressed as [38]:

$$p = 1/\left(1 + e^{-y}\right) \tag{1}$$

where $p$ represents the probability of Fusarium wilt occurrence in this chapter, ranging between 0 and 1, $e$ is the numerical constant, and $y$ refers to the linear combination. They can be expressed in a formula as:

$$y = \beta_0 + \beta_1 x_1 + \beta_2 x_2 + \ldots + \beta_n x_n \tag{2}$$

where $\beta_0$ refers to the intercept, $\beta_i$ and $x_i$ ($i$ = 0, 1, 2, ..., n) are the slope coefficients and independent variables, respectively. The logistic regression models were fitted with the modelling dataset through SPSS 20.0 software (SPSS Inc., Chicago, Illinois, USA) in this section.

Following the model fitting, the validation datasets were used to verify the accuracy of Fusarium wilt identification models, with indicators of the Kappa coefficient and overall accuracy (OA) [39, 40]. The Kappa coefficient ranges between −1 and 1, kappa ≥0.75 represents excellent agreement, 0.75 > kappa ≥0.4 represents fair to good agreement, kappa <0.4 represents poor represents [41]. The OA is the sum of the correctly identified plots divided by the total number of plots.

## 3. Banana fusarium wilt recognition

### 3.1 Statistical characteristics of VIs change after disease infection

**Table 2** shows the VI values of the diseased and healthy sample plots. Significant differences (independent $t$-test) were observed in the NDVI, NDRE, $CI_{green}$, $CI_{RE}$, ARI, and CARI values between the healthy plots and diseased plots ($p < 0.01$), but not observed in the SIPI and $SIPI_{RE}$ values ($p > 0.05$). Hence, we selected NDVI, NDRE, $CI_{green}$, $CI_{RE}$, ARI, and CARI for follow-up analysis.

### 3.2 Recognition model fitting with different VIs

In this section, the relationships between the VIs and the plants infected or uninfected with Fusarium wilt were described by using the BLR method with

| Experiment Site | VI | Sample plot | Mean | Std. Deviation | *p* Value (*t*-test) |
|---|---|---|---|---|---|
| Guangxi site | NDVI | Healthy | 0.54 | 0.11 | 0.00 |
| | | Diseased | 0.34 | 0.14 | |
| | NDRE | Healthy | 0.20 | 0.08 | 0.00 |
| | | Diseased | 0.02 | 0.09 | |
| | SIPI | Healthy | 0.88 | 0.36 | 0.24 |
| | | Diseased | 1.68 | 5.26 | |
| | $SIPI_{RE}$ | Healthy | 0.58 | 0.71 | 0.25 |
| | | Diseased | 2.07 | 9.77 | |
| | $CI_{green}$ | Healthy | 1.08 | 0.32 | 0.00 |
| | | Diseased | 0.43 | 0.33 | |
| | $CI_{RE}$ | Healthy | 0.56 | 0.22 | 0.00 |
| | | Diseased | 0.09 | 0.22 | |
| | ARI | Healthy | 0.85 | 0.15 | 0.00 |
| | | Diseased | 0.62 | 0.16 | |
| | CARI | Healthy | 0.34 | 0.04 | 0.00 |
| | | Diseased | 0.30 | 0.06 | |
| Hainan site | NDVI | Healthy | 0.44 | 0.05 | 0.00 |
| | | Diseased | 0.36 | 0.06 | |
| | NDRE | Healthy | 0.35 | 0.10 | 0.00 |
| | | Diseased | 0.12 | 0.09 | |
| | SIPI | Healthy | 1.07 | 0.07 | 0.06 |
| | | Diseased | 1.18 | 0.12 | |
| | $SIPI_{RE}$ | Healthy | 1.11 | 0.11 | 0.04 |
| | | Diseased | 1.23 | 0.16 | |
| | $CI_{green}$ | Healthy | 0.92 | 0.26 | 0.00 |
| | | Diseased | 0.49 | 0.26 | |
| | $CI_{RE}$ | Healthy | 0.35 | 0.10 | 0.00 |
| | | Diseased | 0.12 | 0.09 | |
| | ARI | Healthy | 0.87 | 0.30 | 0.03 |
| | | Diseased | 0.61 | 0.35 | |
| | CARI | Healthy | 0.43 | 0.16 | 0.01 |
| | | Diseased | 0.33 | 0.19 | |

**Table 2.**
*Statistical characteristics of the VI values of the diseased and healthy sample plots.*

dataset MD. The classification accuracy of the relational models was verified via both dataset VD1 and VD2. It was found that the use of the NDVI, NDRE, $CI_{green}$, and $CI_{RE}$ led to relatively good fitting recognition models with the OA values greater than 80% (**Table 3**). Of all the VIs, $CI_{RE}$ obtained the highest verified OA and Kappa coefficient for both VD1 (91.7% for OA and 0.83 for Kappa) and VD2 (80.0% for OA and 0.59 for Kappa), thereby indicating that $CI_{RE}$ performed best in the identification of Fusarium wilt. It could be seen that those VIs containing red-edge

| VI | Recognition model | Dataset VD1 | | Dataset VD2 | |
|---|---|---|---|---|---|
| | | OA (%) | Kappa | OA (%) | Kappa |
| NDVI | $y = 5.373–11.851 \times NDVI$ | 83.3 | 0.66 | 62.9 | 0.22 |
| NDRE | $y = 1.802–15.775 \times NDRE$ | 87.5 | 0.75 | 65.7 | 0.39 |
| $CI_{green}$ | $y = 3.118–4.144 \times CI_{green}$ | 87.5 | 0.74 | 74.3 | 0.47 |
| $CI_{RE}$ | $y = 1.935–6.110 \times CI_{RE}$ | 91.7 | 0.83 | 80.0 | 0.59 |
| ARI | $y = 5.326–7.247 \times ARI$ | 83.3 | 0.66 | 68.6 | 0.37 |
| CARI | $y = 3.172–9.966 \times CARI$ | 66.7 | 0.35 | 60.0 | 0.21 |

**Table 3.**
*Recognition models of banana fusarium wilt for different VIs.*

band (e.g., NDRE vs. NDVI and $CI_{RE}$ vs. $CI_{green}$) obtained higher verified OA and Kappa coefficients. Nonetheless, CARI and ARI achieved relatively low verified OA and Kappa coefficients.

### 3.3 Recognition model fitting with different resolution images

Evaluating the impact of image resolutions on the accuracy of Fusarium wilt recognition can provide guidance for the large-scale application of satellite-based data. In this chapter, the original UAV images were first resampled to five different spatial resolutions (0.5-m, 1-m, 2-m, 5-m, and 10-m), which were then used for Fusarium wilt monitoring. We calculated both the optimal VI without a red-edge band ($CI_{green}$) and optimal VI with a red-edge band ($CI_{RE}$) at different resolutions. **Table 4** lists the results of Fusarium wilt recognition model for the $CI_{green}$ and $CI_{RE}$ VIs at different resolutions. As indicated by the verified results, the $CI_{RE}$ at resolution 0.5-m, 1-m, and 2-m were all obtained the acceptable verified OA (over 70%) and Kappa coefficients (over 0.40). When using the dataset VD1, the verified OA at resolution 0.5-m, 1-m, and 2-m were 91.7%, 79.2%, and 75.0%, respectively, and the Kappa coefficients were 0.83, 0.60, and 0.53, respectively. When using dataset VD2, the verified OA at resolution 0.5-m, 1-m, and 2-m were 85.7%, 74.3%, and 71.4%, respectively, and the Kappa coefficients were 0.71, 0.48, and 0.41, respectively. Despite that, the OA and Kappa coefficients at resolution 5-m and 10-m resolution were relatively low, and their values dropped as the resolution decreased. Moreover, at the same resolution, the accuracy of the $CI_{green}$-based model for Fusarium wilt recognition was lower than that of $CI_{RE}$-based model. In fact, the only acceptable result for the $CI_{green}$ was at 0.5-m resolution.

### 3.4 Fusarium wilt Banana distribution mapping at different resolutions

With the aim to further explore the visual effects of image resolutions, the distribution of Fusarium wilt infected and uninfected areas at the Guangxi site were mapped using different resolution images. $CI_{RE}$-based and $CI_{green}$-based Fusarium wilt identification models were respectively used to create the Fusarium wilt distribution maps. As can be seen in **Figures 2** and **3**, the maps with 0.08-m, 0.5-m, 1-m and 2-m resolution show quite similar distributions of the occurrence of Fusarium wilt; however, the maps with 5-m and 10-m resolutions exhibited very little detail. **Table 5** lists the area and percentage of the areas infected with Fusarium wilt at different resolutions. For the maps based on $CI_{RE}$ models, the total areas of Fusarium wilt were between 5.69 ha and 6.59 ha, accounting for 38.2% and 44.3% of the

| Resolution | Recognition model | Dataset VD1 | | Dataset VD2 | |
|---|---|---|---|---|---|
| | | OA (%) | Kappa | OA (%) | Kappa |
| $CI_{RE}$ | | | | | |
| 0.5-m | $y = 1.987–5.826 \times CI_{RE}$ | 91.7 | 0.83 | 85.7 | 0.71 |
| 1-m | $y = 1.645–4.896 \times CI_{RE}$ | 79.2 | 0.60 | 74.3 | 0.48 |
| 2-m | $y = 1.475–4.178 \times CI_{RE}$ | 75.0 | 0.53 | 71.4 | 0.41 |
| 5-m | $y = 1.027–2.854 \times CI_{RE}$ | 70.8 | 0.42 | 65.7 | 0.30 |
| 10-m | $y = 0.761–1.817 \times CI_{RE}$ | 62.5 | 0.25 | 62.9 | 0.24 |
| $CI_{green}$ | | | | | |
| 0.5-m | $y = 3.166–3.946 \times CI_{green}$ | 87.5 | 0.75 | 74.3 | 0.48 |
| 1-m | $y = 2.633–3.266 \times CI_{green}$ | 75.0 | 0.51 | 65.7 | 0.32 |
| 2-m | $y = 2.421–2.936 \times CI_{green}$ | 75.0 | 0.51 | 62.9 | 0.26 |
| 5-m | $y = 1.552–1.862 \times CI_{green}$ | 66.7 | 0.35 | 48.6 | 0.01 |
| 10-m | $y = 1.044–1.158 \times CI_{green}$ | 58.3 | 0.18 | 45.7 | −0.01 |

**Table 4.**
*Recognition models of banana fusarium wilt for the $CI_{RE}$ and $CI_{green}$ at different resolutions.*

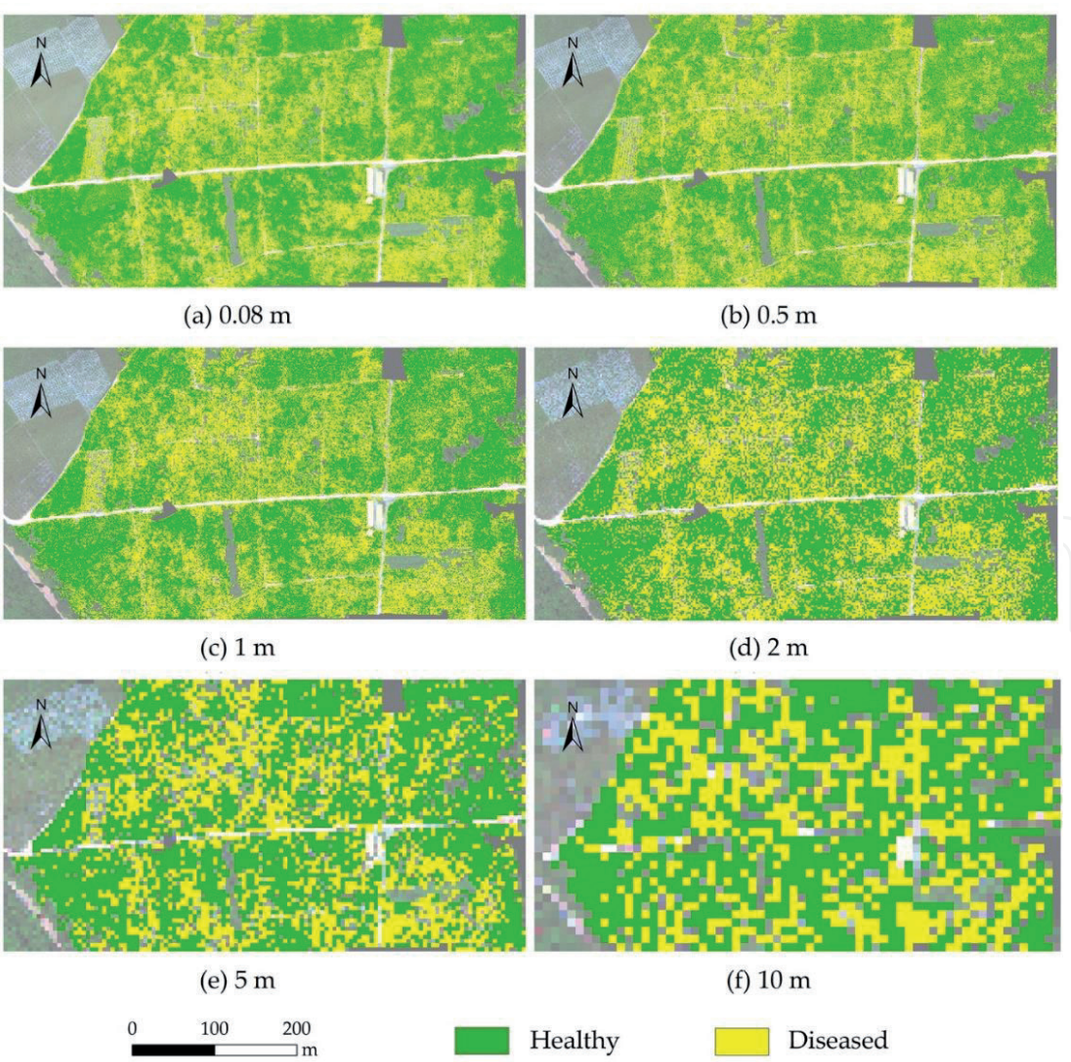


**Figure 2.**
*Maps of the distribution of fusarium wilt based on the $CI_{RE}$ with different resolution images at the Guangxi site.*

banana plantation area. Taking a map with a resolution of 2 m as an example, the incidence of Fusarium wilt is between 40.8% and 43.6%. For the maps based on $CI_{green}$ models, the total areas of Fusarium wilt were between 5.09 ha and 6.63 ha, accounting for 34.2% and 44.6% of the banana plantation area. Among them, the percentages of Fusarium wilt of the 0.08-m and 0.5-m resolution maps were 40.1% and 44.6%, respectively.

### 3.5 Discussion

It was found that among all the VIs used in this chapter, $CI_{RE}$ was the best red-edge VI and $CI_{green}$ was the best non-red-edge VI for Fusarium wilt identification. This is because these two VIs are sensitive to the changes of chlorophyll content of a plant, and Fusarium wilt infection in banana will cause a decrease in leaf chlorophyll content [34, 35, 42]. Furthermore, compared with VIs without the red-edge band, VIs with the red-edge band had higher OA and Kappa coefficients (e.g., NDRE vs. NDVI, and $CI_{RE}$ vs. $CI_{green}$). It has been widely proved that the red-edge position is very sensitive to the changes of the plant chlorophyll content [43, 44]. Nevertheless, the UAV-based multispectral imagery used in this chapter only possessed 5 bands, which still cannot fully characterise the differences of the spectral characteristics between the diseased and healthy plants. It is therefore of great

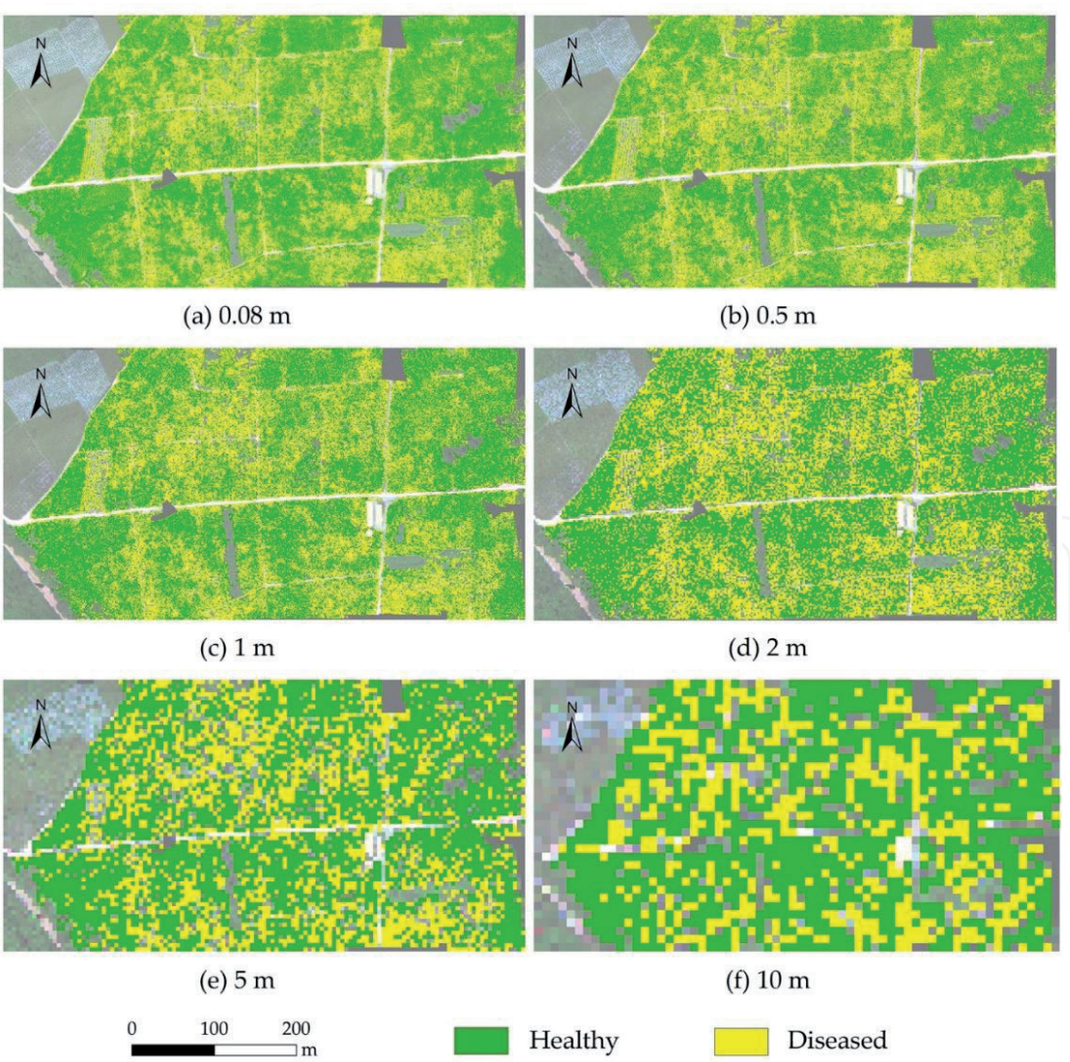


**Figure 3.**
*Maps of the distribution of fusarium wilt based on the $CI_{green}$ with different resolution images at the Guangxi site.*

| Resolution | Diseased area (ha) | Proportion of diseased area (%) |
|---|---|---|
| $CI_{RE}$ | | |
| 0.08-m | 6.04 | 40.8 |
| 0.5-m | 6.59 | 44.3 |
| 1-m | 6.28 | 42.2 |
| 2-m | 6.47 | 43.6 |
| 5-m | 5.70 | 38.5 |
| 10-m | 5.69 | 38.2 |
| $CI_{green}$ | | |
| 0.08-m | 5.95 | 40.1 |
| 0.5-m | 6.63 | 44.6 |
| 1-m | 6.44 | 43.3 |
| 2-m | 6.63 | 44.6 |
| 5-m | 5.69 | 38.4 |
| 10-m | 5.09 | 34.2 |

**Table 5.**
*Areas of fusarium wilt based on the $CI_{RE}$ and $CI_{green}$ with different resolution images at the Guangxi site.*

significance to use hyperspectral data to further study the sensitivity of certain wavebands to banana Fusarium wilt.

The results also showed the potential of combining BLR and VIs to accurately identify Fusarium wilt of banana. Based on this method, an ideal framework for the use of spectral features can be obtained, so as to clarify the pathological mechanisms. In this chapter, the dependent variable was the occurrence of banana Fusarium wilt. Under the circumstance that the predicted variable has a binary nature, BLR can be regarded as a suitable approach [38]. In addition, BLR can deliver better performance than discriminant analysis in the case that the predictor variables are continuous, categorical, or a combination of the two [45]. BLR is highly interpretable, very efficient, and does not require large computational resources, so it is widely used to describe the relationship between a dependent variable and multiple independent variables [38]. Moreover, due to its linear decision surface, non-linear problems cannot be solved by the logistic regression. With the development of artificial intelligence, pattern recognition and machine learning methods will become more common in the use of remote sensing to monitor and predict plant diseases [46].

The Fusarium wilt detection models were verified both using the dataset VD1 VD2. It can be seen from the verification results that both $CI_{RE}$ and $CI_{green}$ performed well in the identification of Fusarium wilt (OA > 70%, and Kappa values >0.4). This indicates that the detection models of Fusarium wilt have a good transferability in other fields. **Tables 3** and **4** show that the Kappa coefficients of the dataset VD2 were lower than those of the dataset VD1, thus indicating that applying the detection methodology of Fusarium wilt in other fields would cause some precision loss. This situation may be due to the following factors. First of all, one of the most important factors affecting the verification results could be the fact that there were two different banana varieties at the experimental sites ("Williams B6" in VD1 and "Baxijiao" in VD2). These showed that there were differences in their biophysical and biochemical characteristics, which may cause differences in spectral characteristic information. Secondly, due to the differences in the planting time and climatic

conditions of the two experimental sites, their growth stages differed greatly. In fact, the banana plants of two experimental areas were at different growth stages during the investigation. Moreover, soil types, planting density, and environmental conditions for crop growth are also important factors that affect the applicability of the Fusarium wilt identification model. Therefore, it is recommended to appropriately optimise the BLR parameters when applying this method in other regions.

In this chapter, the original UAV images were resampled to generate five resolution images (i.e., 0.5-m, 1-m, 2-m, 5-m, and 10-m) to evaluate the impact of different resolutions on the accuracy of Fusarium wilt monitoring. It was found that imagery with a resolution smaller than 2 meters had a good accuracy for Fusarium wilt monitoring, which may be related to the planting spacing and the canopy size of banana. With the reduction of the resolution, the mixed pixel problem influences the precision of object recognition and classification. However, image resolution is not the only difference seen between UAV-based and satellite-based sensors. The wavelength information captured by the satellite-based sensor is different from that of UAV-based sensors. Thus, the simulation results at different resolutions should be further verified with actual satellite-based data. In this chapter, single-period multispectral images were used, which limits the spectral response mechanism to determine the changes in the biophysical and chemical parameters caused by Fusarium wilt. In order to overcome this problem, it is necessary to use multitemporal and hyperspectral images for dynamic monitoring of the occurrence of Fusarium wilt. Additionally, it is also of great value to explore the differences in the spectral response characteristics of Fusarium wilt and other yellowing stresses (i.e., nutrition deficiency and drought stress).

## 4. Conclusions

This research used UAV multispectral images to develop a method for identifying Fusarium wilt of banana. The results revealed that the VIs method with BLR analysis can well identify Fusarium wilt. of all the VIs investigated, the $CI_{RE}$ exhibited the optimal performance, with the OA and Kappa coefficients of 91.7% and 0.83 for dataset VD1 and 80.0% and 0.59 for dataset VD2. VIs that included a red edge band obtained better results than those that did not have one. According to the analysis of different resolutions, a resolution smaller than 2 m produced a good identification accuracy of Fusarium wilt. As the resolution decreased however, the identification accuracy decreased. The results indicate that UAV-based multispectral imagery can be applied to identify Fusarium wilt of banana, thus providing reference for disease treatment and crop planting adjustments.

## Acknowledgements

This research was funded by Hainan Provincial Major Science and Technology Program of China (ZDKJ2019006); Youth Innovation Promotion Association CAS (2021119); Future Star Talent Program of Aerospace Information Research Institute, Chinese Academy of Sciences (2020KTYWLZX08); National special support program for high-level personnel recruitment (Wenjiang Huang).

## Conflict of interest

The authors declare no conflict of interest.

## Thanks

We gratefully acknowledge the National Meteorological Information Center of China, Guangxi Jiejiarun Technology Co., Ltd. and Guangxi Jinsui Agriculture Group Co., Ltd. for the experiments.



## Author details

Huichun Ye[1,2*], Wenjiang Huang[1,2], Shanyu Huang[3], Chaojia Nie[1], Jiawei Guo[1,4] and Bei Cui[1,2]

1 Key Laboratory of Digital Earth Science, Information Research Institute, Chinese Academy of Sciences, Beijing, China

2 Laboratory of Earth Observation of Hainan Province, Sanya, China

3 Chinese Academy of Agricultural Engineering Planning and Design, Beijing, China

4 School of Marine Technology and Geomatics, Jiangsu Ocean University, Lianyungang, China

*Address all correspondence to: yehc@radi.ac.cn

## References

[1] Shen Z, Xue C, Penton C.R, Thomashow L.S, Zhang N, Wang B, Ruan Y, Li R, Shen Q. Suppression of banana Panama disease induced by soil microbiome reconstruction through an integrated agricultural strategy. Soil. Biol. Biochem. 2019; 128: 164-174. http://dx.doi.org/10.1016/j.soilbio.2018.10.016.

[2] Ordonez N, Seidl M F, Waalwijk C, Drenth A, Kilian A, Thomma B P H J, Ploetz R C, Kema G H J. Worse comes to worst: Bananas and Panama disease-when plant and pathogen clones meet. PLoS Pathog. 2015; 11: e1005197. http://dx.doi.org/10.1371/journal.ppat.1005197.

[3] Van den Berg N, Berger D K, Hein I, Birch P R, Wingfield M J, Viljoen A. Tolerance in banana to Fusarium wilt is associated with early up-regulation of cell wall-strengthening genes in the roots. Mol. Plant Pathol. 2007; 8: 333-341. http://dx.doi.org/10.1111/j.1364-3703.2007.00389.x.

[4] Lin B, Shen H. Fusarium oxysporum f. sp. cubense. In: Wan F, Jiang M, Zhan A, editors. Biological Invasions and Its Management in China: Volume 2. Springer Singapore: Singapore, Singapore, 2017.

[5] Shi Y, Huang W, Ye H, Ruan C, Xing N, Geng Y, Dong Y, Peng D. Partial least square discriminant analysis based on normalized two-stage vegetation indices for mapping damage from rice diseases using PlanetScope datasets. Sensors 2018; 18: 1901. http://dx.doi.org/10.3390/s18061901.

[6] Zheng Q, Huang W, Cui X, Shi Y, Liu L. New spectral index for detecting wheat yellow rust using Sentinel-2 multispectral imagery. Sensors 2018; 18: 868. http://dx.doi.org/10.3390/s18030868.

[7] Jin X, Jie L, Wang S, Qi H J, Li S W. Classifying wheat hyperspectral pixels of healthy heads and Fusarium head blight disease using a deep neural network in the wild field. Remote Sens. 2018; 10: 395. http://dx.doi.org/10.3390/rs10030395.

[8] Mahlein A K, Alisaac E, Al Masri A, Behmann J, Dehne H W, Oerke E C. Comparison and Combination of Thermal Fluorescence and Hyperspectral Imaging for Monitoring Fusarium Head Blight of Wheat on Spikelet Scale. Sensors 2019; 19: 2281. http://dx.doi.org/10.3390/s19102281.

[9] Huang W, Lamb D.W, Niu Z, Zhang Y, Liu L, Wang J. Identification of yellow rust in wheat using in-situ spectral reflectance measurements and airborne hyperspectral imaging. Precis. Agric. 2007; 8: 187-197. http://dx.doi.org/10.1007/s11119-007-9038-9.

[10] Huang W, Guan Q, Luo J, Zhang J, Zhao J, Liang D, Huang L, Zhang D. New optimized spectral indices for identifying and monitoring winter wheat diseases. IEEE J. Sel. Top. Appl. Earth Observ. Remote Sens. 2014; 7: 2516-2524. http://dx.doi.org/10.1109/JSTARS.2013.2294961.

[11] Shi Y, Huang W, Gonzalez-Moreno P, Luke B, Dong Y, Zheng Q, Ma H, Liu L. Wavelet-based rust spectral feature set (WRSFs): A novel spectral feature set based on continuous wavelet transformation for tracking progressive host-pathogen interaction of yellow rust on wheat. Remote Sens. 2018; 10: 525. http://dx.doi.org/10.3390/rs10040525.

[12] Yuan L, Pu R, Zhang J, Wang J, Yang H. Using high spatial resolution satellite imagery for mapping powdery mildew at a regional scale. Precis. Agric. 2016; 17: 332-348. http://dx.doi.org/10.1007/s11119-015-9421-x.

[13] Zhao J, Xu C, Xu J, Huang L, Zhang D, Liang D. Forecasting the wheat powdery mildew (Blumeria graminis f. Sp tritici) using a remote sensing-based decision-tree classification at a provincial scale. Australas Plant Path. 2018; 47: 53-61. http://dx.doi.org/10.1007/s13313-017-0527-7.

[14] Dhau I, Adam E, Mutanga O, Ayisi K, Abdel-Rahman E.M, Odindi J, Masocha M. Testing the capability of spectral resolution of the new multispectral sensors on detecting the severity of grey leaf spot disease in maize crop. Geocarto Int. 2018; 33: 1223-1236. http://dx.doi.org/10.1080/10106049.2017.1343391.

[15] Huang J, Liao H, Zhu Y, Sun J, Sun Q, Liu X. Hyperspectral detection of rice damaged by rice leaf folder (Cnaphalocrocis medinalis). Comput. Electron. Agric. 2012; 82: 100-107. http://dx.doi.org/10.1016/j.compag.2012.01.002.

[16] Yang C M. Assessment of the severity of bacterial leaf blight in rice using canopy hyperspectral reflectance. Precis. Agric. 2010; 11: 61-81. http://dx.doi.org/10.1007/s11119-009-9122-4.

[17] Zhang M, Qin Z, Liu X, Ustin S.L. Detection of stress in tomatoes induced by late blight disease in California USA using hyperspectral remote sensin. Int. J. Appl. Earth. Obs. Geoinf. 2003; 4: 295-310. http://dx.doi.org/10.1016/S0303-2434(03)00008-4.

[18] Jones C.D, Jones J.B, Lee W.S. Diagnosis of bacterial spot of tomato using spectral signatures. Comput. Electron. Agric. 2010; 74: 329-335. http://dx.doi.org/10.1016/j.compag.2010.09.008.

[19] Bravo C, Moshou D, West J, McCartney A, Ramon H. Early disease detection in wheat fields using spectral reflectance. Biosyst. Eng. 2003; 84: 137-145. http://dx.doi.org/10.1016/S1537-5110(02)00269-6.

[20] Devadas R, Lamb D.W, Simpfendorfer S, Backhouse D. Evaluating ten spectral vegetation indices for identifying rust infection in individual wheat leaves. Precis. Agric. 2009; 10: 459-470. http://dx.doi.org/10.1007/s11119-008-9100-2.

[21] Deng L, Mao Z, Li X, Hu Z, Yan Y. UAV-based multispectral remote sensing for precision agriculture: A comparison between different cameras. ISPRS J. Photogramm. Remote Sens. 2018; 146: 124-136. http://dx.doi.org/10.1016/j.isprsjprs.2018.09.008.

[22] Dash J.P, Watt M.S, Pearse G.D, Heaphy M, Dungey H.S. Assessing very high resolution UAV imagery for monitoring forest health during a simulated disease outbreak. ISPRS J. Photogramm. Remote Sens. 2017; 131: 1-14. http://dx.doi.org/10.1016/j.isprsjprs.2017.07.007.

[23] Liu B, Shi Y, Duan Y, Wu W. UAV-based crops classification with joint features from orthoimage and DSM data. Int. Arch. Photogram. Remote Sens. Spat. Inform. Sci. 2018; XLII-3: 1023-1028. http://dx.doi.org/10.5194/isprs-archives-XLII-3-1023-2018.

[24] Liu K, Zhou Q B, Wu W B, Xia T, Tang H J. Estimating the crop leaf area index using hyperspectral remote sensing. J. Integr. Agr. 2016; 15: 475-491. http://dx.doi.org/10.1016/S2095-3119(15)61073-5.

[25] Machovina B L, Feeley K J, Machovina B J. UAV remote sensing of spatial variation in banana production. Crop Pasture Sci. 2016; 67: 1281-1287. http://dx.doi.org/10.1071/CP16135.

[26] Ye H, Cui B, Huang S, Dong Y, Huang W, Ren Y, Guo A, Jin Y. Identification of banana Fusarium wilt disease based on UAV multi-spectral

imagery. In: Proceedings of the International Conference on Intelligent Agriculture, Beijing, China, 18-21 October 2019.

[27] Ye H, Huang W, Huang S, Cui B, Dong Y, Guo A, Ren Y, Jin Y. Recognition of Banana Fusarium Wilt Based on UAV Remote Sensing. Remote Sens. 2020; 12: 938. http://dx.doi.org/10.3390/rs12060938.

[28] Li N, Xie G, Zhou D, Zhang C, Jiao C. Remote sensing classification of marsh wetland with different resolution images. J. Resour. Ecol. 2016; 7: 107-114. http://dx.doi.org/10.5814/j.issn.1674-764x.2016.02.005.

[29] IUSS Working Group WRB. World Reference Base for Soil Resources 2006; FAO: Rome Italy 2006.

[30] Rouse J W, Haas R H, Schell J A, Deering D W. Monitoring vegetation systems in the great plains with ERTS. In: Proceedings of the Third ERTS-1 Symposium NASA SP-351, Greenbelt, MD, USA, 10-14 December 1973.

[31] Gitelson A, Merzlyak M N. Spectral reflectance changes associated with autumn senescence of aesculus–hippocastanum L and acer-platanoides L leaves—spectral features and relation to chlorophyll estimation. J. Plant Physiol. 1994; 143: 286-292. http://dx.doi.org/10.1016/S0176-1617(11)81633-0.

[32] Ozdemir A. Using a binary logistic regression method and GIS for evaluating and mapping the groundwater spring potential in the Sultan Mountains (Aksehir Turkey). J. Hydrol. 2011; 405: 123-136.

[33] Ramoelo A, Skidmore A K, Cho M A, Schlerf M, Mathieu R, Heitkonig I M A. Regional estimation of savanna grass nitrogen using the red-edge band of the spaceborne RapidEye sensor. Int. J. Appl. Earth. Obs. Geoinf. 2012; 19: 151-162. http://dx.doi.org/10.1016/j.jag.2012.05.009.

[34] Gitelson A A, Gritz Y, Merzlyak M N. Relationships between leaf chlorophyll content and spectral reflectance and algorithms for non-destructive chlorophyll assessment in higher plant leaves. J. Plant Physiol. 2003; 160: 271-282. http://dx.doi.org/10.1078/0176-1617-00887.

[35] Gitelson A A, Vina A, Ciganda V, Rundquist D C, Arkebauer T J. Remote estimation of canopy chlorophyll content in crops. Geophys. Res. Lett. 2005; 32: L08403. http://dx.doi.org/10.1029/2005GL022688.

[36] Zhou X, Huang W, Zhang J, Kong W, Casa R, Huang Y. A novel combined spectral index for estimating the ratio of carotenoid to chlorophyll content to monitor crop physiological and phenological status. Int. J. Appl. Earth. Obs. Geoinf. 2019; 76: 128-142. http://dx.doi.org/10.1016/j.jag.2018.10.012.

[37] Zhou X, Huang W, Zhang J, Kong W, Casa R, Huang Y. A novel combined spectral index for estimating the ratio of carotenoid to chlorophyll content to monitor crop physiological and phenological status. Int. J. Appl. Earth. Obs. Geoinf. 2019; 76: 128-142. http://dx.doi.org/10.1016/j.jag.2018.10.012.

[38] Lee S, Pradhan B. Landslide hazard mapping at Selangor Malaysia using frequency ratio and logistic regression models. Landslides 2007 4: 33-41. http://dx.doi.org/10.1007/s10346-006-0047-y.

[39] Congalton R G. A review of assessing the accuracy of classifications of remotely sensed data. Remote Sens. Environ. 1991; 37: 35-46. http://dx.doi.org/10.1016/0034-4257(91)90048-B.

[40] Foody G M. Classification accuracy comparison: Hypothesis tests and the

use of confidence intervals in evaluations of difference equivalence and non-inferiority. Remote Sens. Environ. 2009; 113: 1658-1663. http://dx.doi.org/10.1016/j.rse.2009.03.014.

[41] Tuanmu M N, Viña A, Bearer S, Xu W, Ouyang Z, Zhang H, Liu J. Mapping understory vegetation using phenological characteristics derived from remotely sensed data. Remote Sens. Environ. 2010; 114: 1833-1844. http://dx.doi.org/10.1016/j.rse.2010.03.008.

[42] Dong X, Wang M, Ling N, Shen Q, Guo S. Potential role of photosynthesis-related factors in banana metabolism and defense against Fusarium oxysporum f. sp cubense. Environ. Exp. Bot. 2016; 129: 4-12. http://dx.doi.org/10.1016/j.envexpbot.2016.01.005.

[43] Clevers J G P W, de Jong S M, Epema G F, van der Meer F, Bakker W H, Skidmore A.K, Addink E.A. MERIS and the red-edge position. Int. J. Appl. Earth. Obs. Geoinf. 2001; 3: 313-320. http://dx.doi.org/10.1016/S0303-2434(01)85038-8.

[44] Dash J, Curran P J. The MERIS terrestrial chlorophyll index. Int. J. Remote Sens. 2004; 25: 5403-5413. http://dx.doi.org/10.1080/01431160420000274015.

[45] Mathew J, Jha V K, Rawat G S. Application of binary logistic regression analysis and its validation for landslide susceptibility mapping in part of Garhwal Himalaya India. Int. J. Remote Sens. 2007; 28: 2257-2275. http://dx.doi.org/10.1080/01431160600928583.

[46] Lu J, Sun L, Huang W. Research progress in monitoring and forecasting of crop pests and diseases by remote sensing. Remote Sens. Technol. Appl. 2019; 34: 21-32. http://dx.doi.org/10.11873/j.issn.1004-0323.2019.1.0021.